

# Quantum enhanced real-time sensing of protein binding process

Mrunal Kamble,<sup>1,2,\*</sup> Evan Humberd,<sup>3</sup> Tian Li,<sup>3,4,5,†</sup> and Girish S. Agarwal<sup>1,2,6,‡</sup>

<sup>1</sup>*Department of Physics and Astronomy, Texas A&M University, College Station, Texas 77843, USA*

<sup>2</sup>*Institute for Quantum Science and Engineering, Texas A&M University, College Station, Texas 77843, USA*

<sup>3</sup>*Department of Chemistry and Physics, University of Tennessee at Chattanooga, Chattanooga, TN 37403, USA*

<sup>4</sup>*UTC Research Institute, University of Tennessee at Chattanooga, Chattanooga, TN 37403, USA*

<sup>5</sup>*UTC Quantum Center, University of Tennessee at Chattanooga, Chattanooga, TN 37403, USA*

<sup>6</sup>*Department of Biological and Agricultural Engineering, Texas A&M University, College Station, Texas 77843, USA*

(Dated: October 31, 2024)

Analyzing biokinetic processes play significant role in understanding fundamental cellular functions. Many physics based technologies used to study such processes are limited by the shot noise inherent to the coherent states of light. These technologies can greatly advantage by leveraging quantum probes to improve the sensitivity of measurements in cellular biology. Surface Plasmon Resonance (SPR) technique has been used effectively to achieve label-free, real-time measurements of protein binding kinetics that constitutes an important biological phenomenon occurring near the cell membrane. Here, we demonstrate the integration of this technique with the two-mode bright squeezed state having fewer fluctuations as compared to the coherent state to improve the sensitivity of measurement in studying a protein binding process. We show 4dB of squeezing as we record the signal-to-noise ratio as the function of time and is maintained throughout the binding process. The quantum advantage as shown in terms of squeezing is achieved despite the total absorption of 74% from the source until the final detection after the sensor. Overall we provide the most practical setup for improving the sensitivity of the time-dependent measurements involved in various biological processes at the molecular level.

## I. INTRODUCTION

Quantum sensing and metrology is a promising field proving its importance by improving the sensitivity of measurements in various fields ranging from phase shift measurements, force measurements, imaging, spectroscopy and more. It has been demonstrated that the current biosensing technologies can greatly advantage by leveraging quantum probes such as the entangled photon sources and squeezed states of light. It is possible to even reach the Heisenberg limit which is fundamental theoretical limit provided by quantum theory to enhance the spatial and temporal resolution in the field of bioimaging [1]. One specialized sub-area of quantum sensing combines the benefits of both the worlds, quantum mechanics and the plasmonic technology [2–4] useful in studying fundamental biochemical processes occurring at the cellular level. There exists many other technologies such as Super-resolution fluorescence microscopy [5] that involves labelling of the specific cellular components with fluorescent dyes, Total Internal Reflection–Fluorescence Correlation Spectroscopy (TIR-FCS) [6, 7] to observe events near the cell surface, nanoplasmonic biosensors [8–10] involving metallic nano-films or nano-structures (mainly gold), among others pushing the limits to improve the sensing capabilities for the molecular level study of the cellular processes.

However, the Surface Plasmon Resonance (SPR) has

proved to be a powerful technique in medical research mainly used to analyse events at or near a metal-dielectric interface, where the metal is typically gold film or nanoparticles and the dielectric constitutes the analyte under study [11–13]. It has been used effectively to achieve label-free, real-time measurements of protein binding kinetics which constitutes an important dynamic process occurring near the cell membrane [14–16]. The SPR technique is based on sensing the minute changes in refractive index  $\Delta n$  of the sample which in turn gives information about concentration, affinity and the kinetic parameters of the protein binding event. Understanding the dynamic processes such as protein binding is essential in learning how diseases develop at the molecular level and finding the potential treatment strategies [17]. Protein binding plays an important role in the area of drug design and delivery and studying this process requires more sophisticated tools to advance the field of medical research [18–21].

Most of the current bio-sensing techniques including SPR systems use coherent source of light for which the sensitivity of measuring the refractive index  $n$  is such that  $\Delta n \propto \frac{1}{\sqrt{N}}$ , where  $N$  is the total number of photons interacting with the sample. This is called the Shot Noise Limit (SNL). It has been shown that the performance of SPR technique is highly dependent on the noise characteristics of the light and that the SPR sensors are reaching their theoretical limit [22–24]. One of the ways to improve the sensitivity of measurements is by increasing the number of photons. However this might not be always feasible due to the common issue of photo-damage where higher intensities of light might destroy or alter the sample under study [25]. An effective way to

\* mrunal@tamu.edu

† tian-li@utc.edu

‡ girish.agarwal@ag.tamu.edu

improve the signal-to-noise ratio (SNR) is by reducing the noise and this is where quantum probes prove extremely useful. Marino et al. demonstrated quantum enhancement of 56% when compared with the corresponding classical configuration of state-of-the-art plasmonic sensor[26] using the squeezed light. Recently, it is extended to apply for an array of sensors simultaneously or measure multiple parameters independently[27]. A theoretical study by Mpofo et al. compares the advantage of using different quantum probes specifically for the Surface Plasmon Resonance (SPR) sensing technique [28]. A recent study by the same group utilizes the single photons generated via Spontaneous Parametric Down Conversion (SPDC) to probe the protein binding kinetics using the SPR sensor[29, 30]. Thus improving the SNR is the key to improving the sensitivity of current technology.

In our work we consider the Two Mode Bright Squeezed State (TMBSS) because of its continuous wave nature allows for a higher number of photons as compared to the discrete quantum sources while still maintaining the quantum correlations between the two modes. It can enhance the sensing capabilities specifically by reducing the fluctuations associated with the intensity difference signal. Pooser et al. has demonstrated a quantum plasmonic sensor using the Kreschmann configuration and the TMBSS source to measure the shift in SPR dip for samples with different refractive index [31]. However, no previous study has experimentally investigated the quantum advantage of TMBSS in the context of time dependent SPR sensing to measure the protein binding affinities, association rates, and dissociation rates.

In this paper, we present the most practical setup to integrate the TMBSS along with the SPR sensor and give proof of principle experiment showing the quantum advantage which stays almost constant throughout the protein binding process. This setup can be used to measure the kinetic parameters with higher precision than its classical counterpart when working in the shot noise limited region. We first explain in detail the workings of the SPR sensor that detects minute changes in the refractive index of the sample in contact with the gold film. The sensitivity of measurement of refractive index is directly related to the sensitivity of measuring the kinetic parameters. We then explain the noise reduction achieved using the TMBSS in the form of squeezing. We describe the experimental setup along with the data processing performed to measure the SNR. We present our findings from plotting the SPR dip useful in deciding the incident angle on sensor to quantifying the SNR as a function of time as the BSA protein binds to the gold film on the sensor. Finally we comment on the challenges as well as the future scope for the setup described in this study.

## II. SCHEMATICS OF THE QUANTUM ENHANCED SURFACE PLASMON SENSOR

Surface Plasmon Resonance is a well-known technique in the field of bio sensing. It is based on the phenomenon where the surface plasmon (electron oscillations) at the metal-dielectric interface gets coupled with the evanescent wave generated due to an incident electromagnetic field [32]. This results in the formation of Transverse Magnetic (TM) wave confined to the metal-dielectric interface called as the Surface Plasmon Polariton (SPP) wave. Although the phenomenon could be observed using different coupling arrangements, the most common setup used is the Kreschmann geometry as shown in Fig 1a. Here the prism, the gold film, and the dielectric medium form the apparatus useful in sensing the refractive index of the dielectric. The SPP wave propagates along the x-axis and decays exponentially on both sides of the interface along the z-axis as shown in Fig 1a. The phase matching conditions necessary for the coupling between the evanescent wave and the surface plasmon could be understood using the dispersion relation for the surface plasmon given by,

$$k_x = \frac{\omega}{c} \sqrt{\frac{\epsilon_2(\omega) * \epsilon_3(\omega)}{\epsilon_2(\omega) + \epsilon_3(\omega)}} \quad (1)$$

where,  $\epsilon_2(\omega)$  is the dielectric function for the metal (here gold) and  $\epsilon_3(\omega)$  is the complex dielectric function for the sensing medium (BSA solution). The real part for the  $\epsilon_2$  for gold is a negative value. Considering Eq. (1), if the incident field is coming from air  $K = \frac{\omega}{c}$  the electric field will not be able to couple with the charge density oscillations since,  $k_x > K_x$ . The use of the prism facilitates this coupling due to the phenomenon of Total Internal Reflection (TIR) which gives rise to the evanescent field

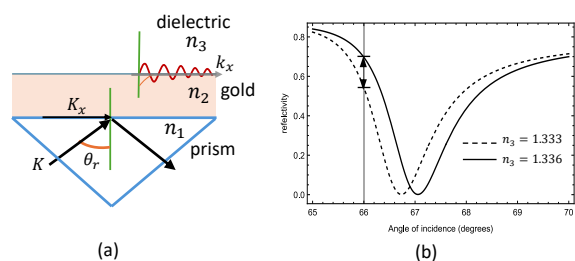


FIG. 1. (a) Kreschmann geometry - The Total Internal Reflection at the prism-metal interface generates an evanescent field on the other side which couples with the charge density oscillations under the right conditions. For a given frequency of laser ( $\omega$ ) and the given gold thickness ( $h$ ), there is a resonant incident angle  $\theta_r$  at which the SPPs absorb the maximum energy giving the characteristic absorption dip. This angle is sensitive to the refractive index. (b) Numerical simulation for SPR absorption dip where the reflectivity of the prism is plotted against the angle of incidence. Small increase in refractive index shifts the absorption dip towards right.

which penetrates through the metal and couples with the surface plasmon thus giving rise to the SPPs. The dispersion relation for the incident field now is given by,

$$K_x = \frac{n_1 \omega}{c} \sin \theta \quad (2)$$

where,  $n_1$  is the refractive index of the prism. Thus the condition for the SPR is given by equating Eq. (1) and Eq. (2),

$$n_1 \sin \theta_r = \sqrt{\frac{\epsilon_2(\omega) * \epsilon_3(\omega)}{\epsilon_2(\omega) + \epsilon_3(\omega)}} \quad (3)$$

Thus, at a particular angle of incidence  $\theta_r$  after the critical angle the SPP are formed leading to the absorption of energy from the incident field. This is called the Surface Plasmon Resonance angle. As we plot the reflectivity of this sensor against the angle of incidence, we can see an absorption dip at the angle of resonance. Thus excitation of the SPP wave is highly sensitive to the refractive index of the dielectric medium at the interface. If we keep the thickness of the metal and the frequency of the laser constant, even the slightest change in the refractive index of the sample can be detected using the shift in the resonance dip. This is shown by the plot in Fig 1b which is based on the theoretical framework of electromagnetic wave propagating through a homogeneous film situated between two semi-finite media as explained in detail in the appendix section.

This technique is already used to study molecular interactions and other parameters useful for bio-sensing. It can be used to measure the affinity of a particular sample, its concentration, specificity as well as the rate of interaction. Here we use this method in studying the rate at which the protein binds the gold film which serves as a preliminary proof of concept that could be extended to study other bio kinetic processes. If we lock the angle of incidence on the left side of the absorption dip, the changes in  $n_3$  as the protein binds to the gold, could be detected by plotting the change in reflectivity as a function of time. This in turn could be translated to find the rate of the association and the dissociation of the protein as it binds and unbinds from the gold surface.

Although an established technique, any protein binding parameter measured using a coherent source of light is shot noise limited. Even When all the technical noise is removed, the shot noise that is inherently related to the photon statistics limits the ability to distinguish two signals within a certain range limited by the fluctuations associated with the signal. The precision of the measurement of parameters studied in the protein binding analysis could be improved by using quantum probes such as the TMBSS source instead of the coherent source. Next we elaborate on the quantum advantage of using TMBSS light.

The two-mode bright squeezed state referring to the intensity difference squeezing is a well-known quantum state that has fewer fluctuations as compared to the coherent state. It could be generated using different non

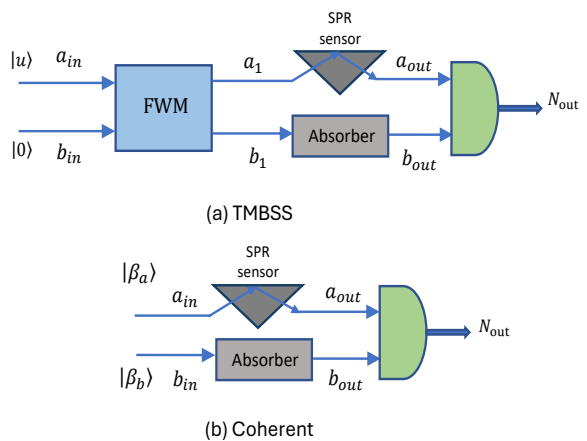


FIG. 2. a. Schematics of Surface Plasmon Resonance sensor using TMBSS light. The probe beam passing through the sensor undergoes an absorption due to SPP and the output Heisenberg operator is denoted by  $a_{out}$ . The conjugate beam intensity is adjusted according to the probe using an absorber and the associated Heisenberg operator is denoted by  $b_{out}$ . The resulting photo current is subtracted and constitutes the signal for the experiment given by  $\langle N_{out} \rangle = \langle a_{out}^\dagger a_{out} - b_{out}^\dagger b_{out} \rangle$ . b. Schematics of SPR sensor using coherent light replicating the experimental conditions for probe and conjugate.

linear process with atomic systems [33] being the most common. Here we use a Rubidium atomic vapour as a non-linear medium in which a coherent field and a vacuum field interact via the Four Wave Mixing (FWM) process to generate two quantum correlated beams namely the probe and the conjugate. As shown in Fig 2a. the two-mode bright squeezed state which ideally can be described as two single modes is defined using the Heisenberg picture given by the equations,

$$\begin{aligned} a_1 &= a_{in} \cosh r + b_{in}^\dagger \sinh r, \\ b_1 &= b_{in} \cosh r + a_{in}^\dagger \sinh r. \end{aligned} \quad (4)$$

where  $r$  is the squeezing parameter and the  $a_1, a_{in}, a_{out}$  being the Heisenberg operators representing the electromagnetic field propagation as described in Fig 2a. The  $r$  parameter in the context of the FWM process is related to the gain parameter  $g$  such that,

$$g = \cosh^2 r \quad (5)$$

where  $g$  is the ratio of the output probe intensity  $\langle a_1^\dagger a_1 \rangle$  and the input seed probe intensity  $\langle a_{in}^\dagger a_{in} \rangle$ . Notice that the input modes, the coherent state  $|u\rangle$  and the vacuum state  $|0\rangle$  are the single modes. Using the balanced detection technique as described in [34], the signal is given by  $\langle N_{out} \rangle = \langle a_{out}^\dagger a_{out} - b_{out}^\dagger b_{out} \rangle$  and the associated fluctuations are given by  $\Delta N_{out} = \sqrt{\langle N_{out}^2 \rangle - \langle N_{out} \rangle^2}$ .

Thus the quantum advantage here could be expressed in terms of the squeezing which is the measure of reduction in noise in dB. It is defined as,

$$S(r) = -10 \log_{10} \left( \frac{(\Delta N_{out})_{TMBSS}^2}{(\Delta N_{out})_{Coh}^2} \right) \quad (6)$$

where,  $(\Delta N_{out})_{Coh}^2$  and  $(\Delta N_{out})_{TMBSS}^2$  are the variance of the TMBSS and the coherent signal respectively.  $(\Delta N_{out})_{Coh}^2$  is measured based on the classical sensor configuration as shown in Fig 2b.

To maintain the squeezing conditions before and after the sensor we match the absorption on the conjugate beam with that on the probe. Next we explain the experimental set up in detail used to study the protein binding process as an example of a biokientic process using the Two Mode Bright Squeezed State as well as using the coherent state.

### III. EXPERIMENTAL SET UP

The experimental setup we used for the quantum-enhanced protein binding analysis can be divided into three parts. Firstly we generate the two mode bright squeezed state using a non-linear process occurring inside a cell containing the Rb85 atomic vapour. This process generates two beams namely the probe and the conjugate that are quantum correlated. In the next step the probe beam passes through the Surface Plasmon Resonance (SPR) sensor where the light matter interaction at the sample-sensor interface enables the study of protein binding process. In the final step, the data is collected using the balanced detection method as theoretically described in the previous section. Each step is further explained below.

#### A. Generating Two-Mode Bright Squeezed State

To generate the Two Mode Bright Squeezed State we use a  $\chi^{(3)}$  process called degenerate Four Wave Mixing (FWM) in which annihilation of two photons of same frequency leads to the creation of two new photons of slightly different frequencies. This non-linear process occurs inside the Rb85 atomic vapour contained in a 2.5 cm long cylindrical vapor cell. The atomic ensemble serves as a non-linear medium where the  $D_1$  line corresponding to the  $5S_{1/2} \rightarrow 5P_{1/2}$  transition including the hyper fine structure of the Rb85 atom constitutes a double- $\Lambda$  energy level configuration as shown in Fig 3b.

As shown in the upper half portion of Fig 3a, we use a continuous wave laser of  $\lambda = 795nm$  which is split into two beams. One of them is used as a strong pump of  $450mW$  to drive the FWM process and the other is used as a seed probe which is a cross-polarized weak beam of  $150\mu W$  to enhance the FWM process. As explained in Fig 3b, this process requires tuning of both the frequencies where the phase matching condition given by

$2\omega_P = \omega_{Pr} + \omega_{Cj}$  along with the momentum conservation condition is satisfied the Rubidium cell. The pump frequency  $\omega_p$  is  $\Delta$  detuned from the Doppler broadened excited state which drives the atom from  $f=2$  to the  $f=3$  ground state via stokes scattered photon of frequency  $\omega_{Pr}$ . Similarly, when another pump photon drives the atom back into the  $f=2$  ground state the anti-stokes scattered photon is generated with frequency  $\omega_{Cj}$ . This process is enhanced by the usage of the seed probe with the frequency  $\omega_{Pr} = \omega_p - (\nu_{HF} + \delta)$  where  $\nu_{HF}$  is the hyper fine splitting of the electronic ground sate and  $\delta$  is the two photon detuning as shown in the energy level diagram.

Single photon detuning  $\Delta$  is achieved by locking the main laser by approximately 1 GHz away from the absorption dip recorded using a reference Rb cell. The Two-photon detuning  $\delta$  on the seed probe frequency is achieved by using a double pass AOM of 1.52 GHz.  $\delta$  ensures that the time lag between probe and conjugate is very small. The momentum conservation is taken care of by carefully aligning the pump beam and the weak probe beam using appropriate mirror arrangements. Another important parameter necessary for FWM process is the temperature of the cell. The cell window is maintained at around 110 degrees whereas the core temperature is maintained around 90 degrees such that the Rb atoms are contained at the center of the cell to ensure maximum photon atom interaction. This leads to the simultaneously generated, equally polarized probe and the conjugate photons that share quantum correlations and are referred to as being in the Two-Mode Bright Squeezed State.

Thus, all the four control parameters namely the single photon detuning, two photon detuning, the pump, probe alignment, and the temperature of the cell are optimized to achieve the squeezing of 7.8 dB as measured at the source just after the cell. Please refer[33, 35–37] for more details of generating the TMBSS source using FWM in Rb85 atomic vapour. The flip mirrors in Fig 3a, create a path for the classical beam which technically is the seed probe diverted just before entering the Rb cell. The further arrangements constitute the application of the twin beams in studying the protein binding process.

#### B. Applying TMBSS to the SPR sensor

At the output of the Rb85 cell, we have three beams namely the probe, the conjugate, and the residual pump. As shown in Fig3a, the residual pump is sent to the beam dump using the Glan Taylor beam-splitter which has the extinction ratio of  $2 \times 10^5 : 1$ . The twin beams are then aligned and collimated ready to be used along with the SPR sensor to study the protein binding process.

We prepared the sensor using the BK7 ( $n=1.51$ ) right angle prism from Thorlabs, a microscope glass slide with 50 nm gold layer (SKU: AU.0500.ALSI) bought from Platypus technologies, and the customized flow cell de-

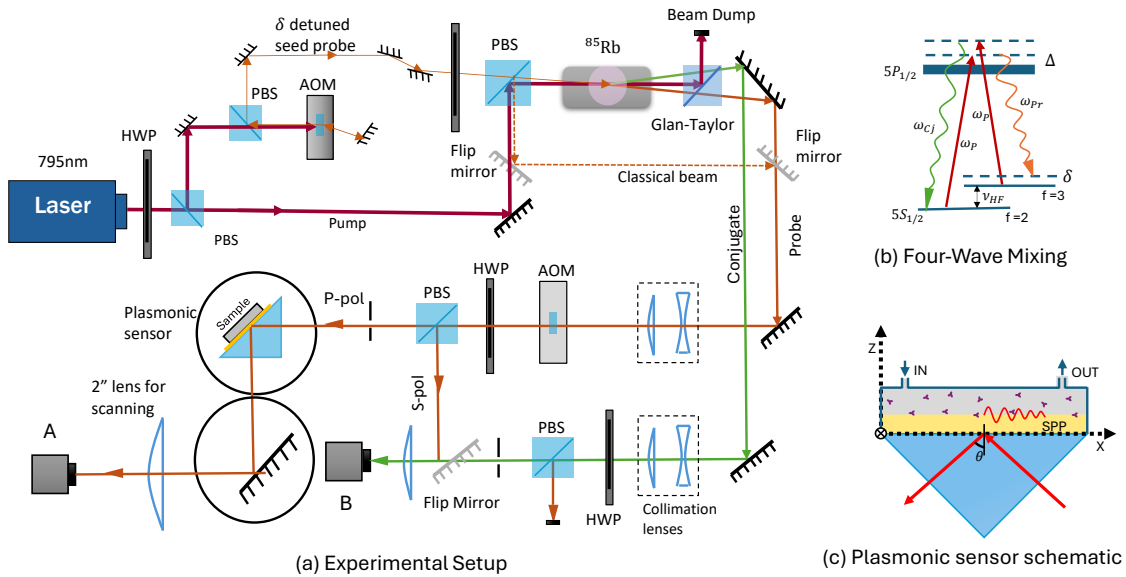


FIG. 3. (a) Experimental setup showing the TMBSS generation using the Rubidium vapor and its application to study protein binding process using SPR sensor. (b) The  $\chi^{(3)}$  FWM process inside a Rb85 atom (c) Schematic of the flow cell and the sensor arrangement.

signed and fabricated using on campus 3D printing facility. As shown in Fig 3c, the sample delivery system needs to work such that the proteins get in contact with the gold without leaking from the flow cell. We use O-ring to avoid any leakage from the flow cell as it is tightly clamped against the microscope slide and the prism. The input and the output ports of the flow cell are connected to a peristaltic pump to control the flow of the sample. Another challenge during the clamping process is the formation of air bubbles between the glass slide and the prism. We use immersion oil (56822-50ml Sigma Aldrich,  $n=1.5$ ) to avoid any air bubbles. We chose the refractive index of the glass of the portion of the microscope slide same as the refractive index of prism as well as the immersion oil such that there is no refraction at the gold dielectric interface.

The sensor is installed on a rotation stage such that the reflectivity can be measured at different incident angles. As shown in the lower half of Fig3a, the probe beam passes through a half wave plate and the PBS so that only the p-polarized light is incident on to the sensor. We place an Acousto-Optic Modulator (AOM) in the probe path, which modulates the intensity to fluctuate at the frequency of 2MHz. This serves as the signal for the experiment. This is an important step to be able to read the signal as well as the noise on the same plot after data processing as explained in the next section. The conjugate beam which is used as a reference, passes through the half-wave plate and the PBS to match the absorption in the probe path. Both the beams are focused on two separate PDA10A2 fixed gain Si detectors from Thorlabs.

### C. Detection and data processing

The data was collected using only the oscilloscope and was post processed with MATLAB. Each detector is connected to two channels on the oscilloscope collecting the AC voltage as well as the DC voltage data. We used the DC data mainly to see the absorption dip for water and to visualize the change in absorption during the protein binding process. The AC data which records the fluctuations in the signal as a function of time was converted into frequency domain using the FFT (Fast Fourier Transform) function in MATLAB. This data is used to find the twin beam noise as well as the Shot Noise Level at different points after the Rb cell. The twin beams undergo an absorption of  $\alpha_1 = 0.08$  at the window of the cell. The difference between the two noise power as measured right after the cell at point A as shown in 4b was 7.8 dB. Next, the twin beams need to pass through a series of optics before reaching the SPR sensor. Here it loses another 38% of the intensity along with the 20% loss at an off resonance angle inside the sensor giving total absorption  $\alpha_2 = 0.5$ . The available squeezing at the wings of the absorption dip is around 4.5 dB as measured after the sensor at point B. Finally, we measure the squeezing after the sensor at point B as we lock the incident angle where the reflectivity of the prism  $r$  is 0.46 ( $\alpha = 0.54$ ). This also constitutes a starting point for the protein binding process. Thus for absorption of  $\alpha_2 = 0.71$  we find the squeezing to be around 4dB. Using the data for the noise (both coherent as well as TMBSS) and the AOM modulation as signal we measure the signal to noise ratio as a function of time. As shown in Fig 5 the peak amplitude is

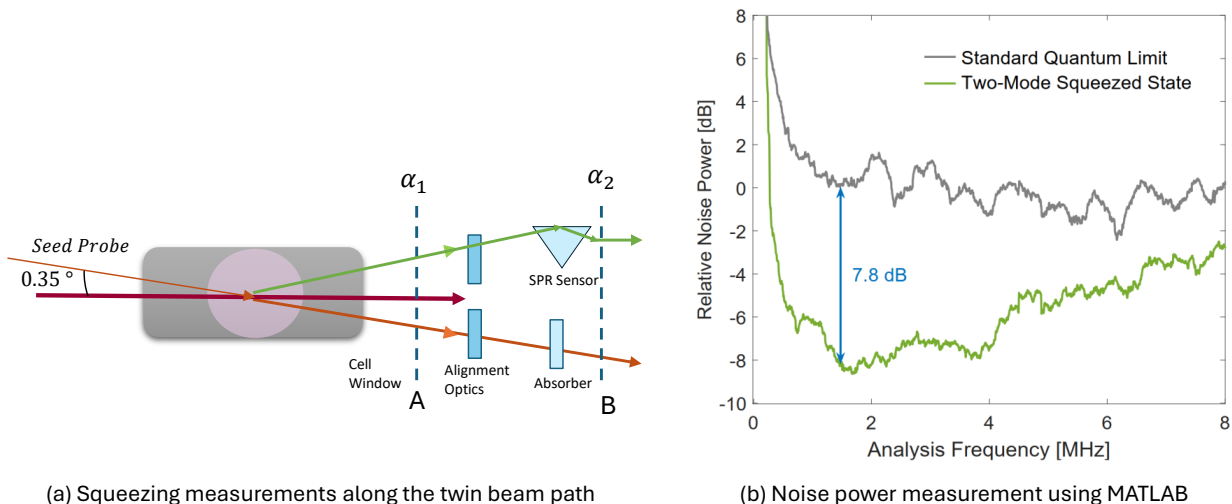


FIG. 4. (a) Squeezing measurements along the propagation path of the twin beams. (b) The difference in the Standard Quantum Limit and the twin beam noise as measured at point A after post-processing the data using MATLAB

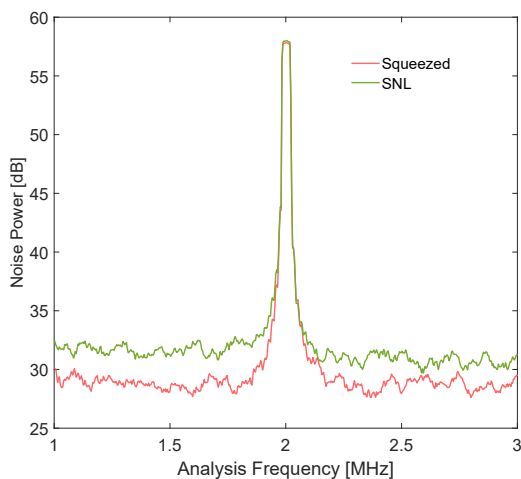


FIG. 5. AOM modulation to see the signal as well as noise on the same plot

taken as the signal and the side bands correspond to the noise for a particular absorption coefficient of the sample. It has been seen before [31] that using the amplitude of the AOM modulation as the signal which is associated to the intensity difference allows us to see the signal and the noise on the same plot plus it helps in removing the technical noise. This forms the complete setup to collect the data involved in studying the biokinetic processes using the Two-Mode Bright Squeezed State along with the Surface Plasmon Resonance sensor.

#### IV. RESULTS

Firstly, we found the Surface Plasmon Resonance (SPR) angle for deionized water ( $n=1.33$ ) by plotting the reflectivity of the sensor against the incident angle using a coherent source. The sensor was aligned such that the classical beam in the probe path is incident at 45 degrees at the gold-prism interface and reflects at a right angle to the incident beam. We fix this position using two irises on the reflected path as a reference point. We recorded the reflectivity of the sensor against the incident angle  $\theta$  as shown in Fig 6a. We collected the data in the range of  $\phi = 29^\circ - 35^\circ$  to the normal of the outer surface of the prism with increments of  $0.2^\circ$ . This gives the incident angle at the gold-prism interface as  $63.72^\circ - 69.63^\circ$ . We find that the intensity reaches its minimum at an angle of  $66.02^\circ$  ( $\theta_r$ ) at which point around 90% of the intensity is absorbed by the excited SPPs. This is in accordance with the theoretical expectations as shown in Fig 1b. The data on the X-Axis was converted into the normalized scale for better comparability with the rest of the plots. Fig 6a helps decide the angle at which we should fix the angle to realize the maximum change in reflected intensity with a minimum shift in the refractive index.

Next, we lock the angle at  $\phi = 32$  degrees which is 0.8 degrees left of the resonance angle  $\theta_r$  corresponding to absorption  $\alpha = 0.59$  or the reflection coefficient  $r = 0.41$ . We then filled the cavity with 10% BSA solution and recorded the change in reflectivity as the protein binds the gold film while changing the refractive index of the sample. As mentioned earlier the angle of resonance shifts towards the right as the refractive index increases, which happens because of the protein binding process. Thus, fixing the angle on the left side of the dip results in an increase of the reflected intensity as the

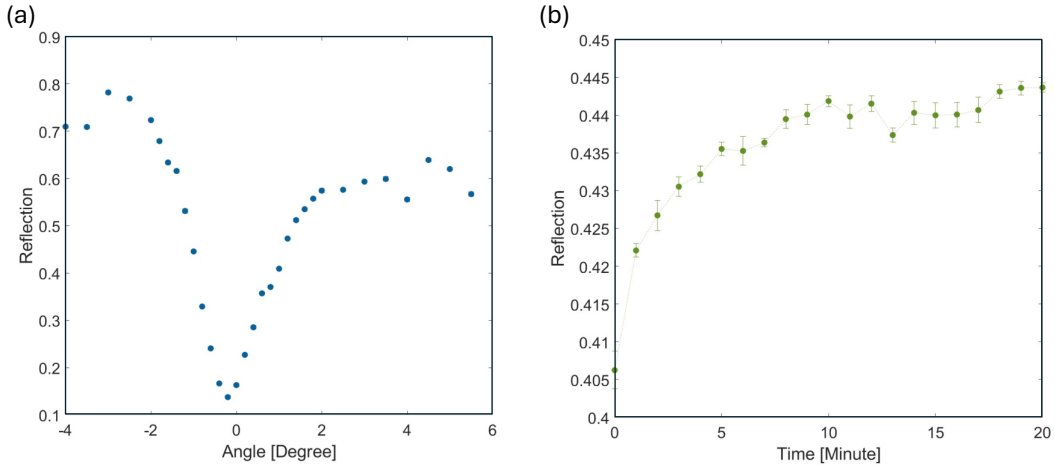


FIG. 6. (a)SPR absorption dip (Classical) (b)Protein binding curve (Classical)

protein binds. This could be visualized in Fig 6b, where the reflected intensity slowly increases with time and the slope of the curve gives the rate of binding. The error bars in the plot correspond to 10 consecutive readings taken at the same time stamp.

Another important parameter helpful in deciding the angle is squeezing. Squeezing in dB as defined by Eq. (6) depends on the absorption that changes at different incident angles on the SPR sensor as shown in Fig7. We experimentally collected the Noise power at different angles around the absorption dip and compared it with the SNL at each point. The SNL was recorded for one angle and using the linear relation of the noise of the coherent source  $(\Delta N)^2 \propto \langle N \rangle$  we calculated the SNL for the rest of the points. As shown in Fig 7a, we get squeezing of around 4 dB at an angle of 0.8 degrees left of  $\theta_r$  as decided using the classical SPR dip data. The squeezing as a function of reflectivity is reported in Fig7b.

Finally, we plot the data for the protein binding process using the reflectivity of the probe beam of the TMBSS source. This plot is shown in fig 8a. As the protein binds, the signal increases due to the shift in SPR dip towards the right increasing the reflectivity similar to the coherent source. While taking the data, we change the conjugate manually by the same proportion as the probe. It more or less ensures that we have the same absorption on conjugate as the probe. Thus we ensure that we get the maximum quantum advantage possible at that absorption level.

It is easier to see the quantum advantage in the SNR plot as a function of time reported in fig 8b. The quantum advantage here is defined as,

$$QA = 10 \log_{10} \left( \frac{(SNR)_{TMBSS}}{(SNR)_{Coh}} \right) \quad (7)$$

The quantum advantage of the TMBSS light is realized when we take the intensity difference between the probe and the conjugate. The signal in this plot is the amplitude of the modulated peak at 2MHz and the noise

is quantified by taking the average of the side bands as shown in Fig 5. We can see the quantum advantage of 4dB despite the total absorption of  $\alpha = 0.74$ . The SNR for TMBSS looks flat because of a very small change in absorption. This plot demonstrates the quantum advantage of using TMBSS in applications involving biokinetic processes.

## V. CONCLUSION

In summary, we have demonstrated the quantum advantage of using Two Mode Bright Squeezed State (TMBSS) in improving the sensitivity of a Surface Plasmon Resonance (SPR) based sensor to study biokinetic processes. We used the protein – Bovine Serum Albumin (BSA) binding to the gold film on the sensor as an example of such biokinetic process. As the protein binds, the reflectivity of the sensor goes up due to the shift in surface plasmon resonance angle. We showed 4dB of squeezing (difference between the coherent source noise and the twin beam noise) as we recorded the signal-to-noise ratio as the function of time and is maintained throughout the binding process. The quantum advantage as shown in terms of squeezing is achieved despite the total absorption of 74% from the source until the final detection after the sensor.

Our work reinforces the utility of TMBSS source highlighting its primary advantage: the continuous variable nature as opposed to the single photon sources that allows for a greater number of photons while still employing the quantum mechanical benefits that arise from the intensity difference squeezing. TMBSS constitutes a readily available quantum probe which is better than the coherent source because of its sub-shot noise characteristic thus allowing for lower intensities with comparable results, making it more gentle to the biological samples. One of the of the main challenges we encountered in the implementation of this technology was the stabilization

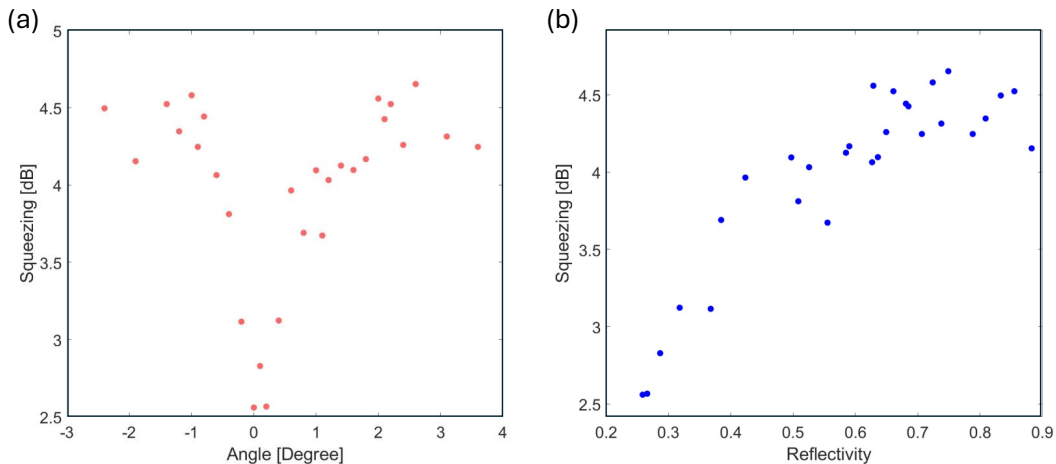


FIG. 7. (a)Squeezing as a function of incident angle following the SPR dip.(b)Squeezing as a function of reflectivity.

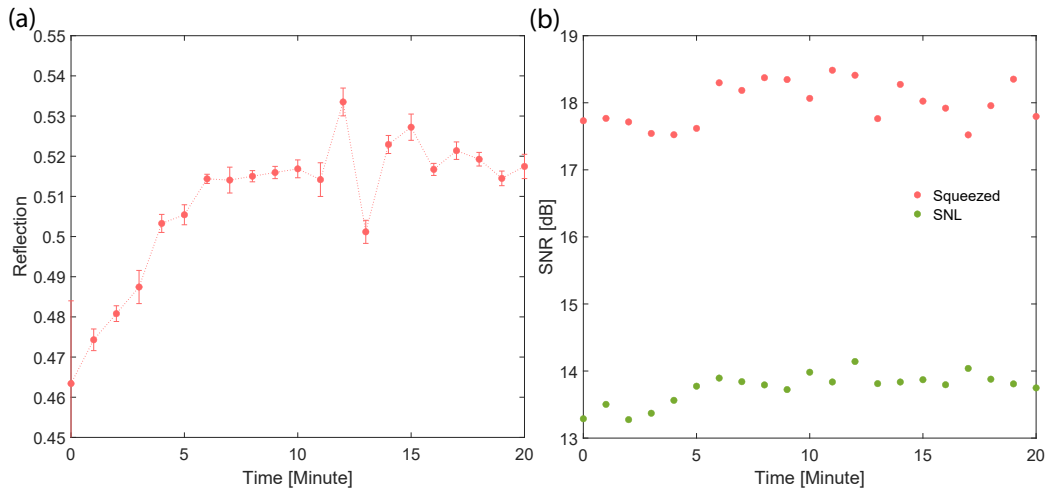


FIG. 8. (a)BSA binding with TMBSS (Quantum) (b)SNR comparison between classical and quantum

issue with the twin beams. Thus, if the source is stabilized and when the both the beams are controlled in such a way that the ratio between probe and conjugate stays the same, this study can be extended to measure the rate of protein binding with higher precision than current technique involving a coherent source. It can also be used to study protein-protein, protein-ligand binding processes that are very significant in the field of biochemistry and biophysics.

Overall, this project brings together two state-of-the-art techniques and provides a most practical, quantum-enhanced SPR setup for improving the sensitivity of time-dependent measurements in the study of biological processes.

## ACKNOWLEDGMENTS

The authors are grateful for the support of the Air Force Office of Scientific Research (Award No. FA-9550-20-1-0366) and the Robert A. Welch Foundation (A-1943-20210327). The final measurements for the SNR were done in the quantum sensing lab at the University of Tennessee at Chattanooga (UTC). We wish to acknowledge the technical help provided by Charles Wallace at Texas A&M University.

## APPENDIX

The numerical simulation in Fig 1b is based on the following theoretical framework.

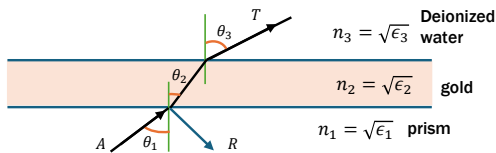


FIG. 9. Propagation of EM wave through homogeneous film situated between two homogeneous media.

The characteristic matrix  $M'$  of the stratified medium here gold film bounded by two semi-infinite media on both sides as shown in Fig 9 evaluated at the gold-prism interface is given by,

$$M' = \begin{bmatrix} m'_{11} & m'_{12} \\ m'_{21} & m'_{22} \end{bmatrix} = \begin{bmatrix} \cos \beta & -\frac{i}{q_2} \sin \beta \\ -iq_2 \sin \beta & \cos \beta \end{bmatrix}$$

where,

$$\beta = h \sqrt{\epsilon_2 \left(\frac{\omega}{c}\right)^2 - \epsilon_1 \left(\frac{\omega}{c}\right)^2 \sin^2 \theta_1}$$

and

$$q_l = \frac{\sqrt{\mu_l}}{\sqrt{\epsilon_l}} \cos \theta_l, \quad \text{For (TM wave)}$$

Here,  $\epsilon_l$  is the dielectric permittivity of the medium  $l=1,2$ ,  $h$  is the thickness of the gold film and  $\omega$  is the frequency of the incident field. In our calculations, the magnetic permeability  $\mu_l$  is considered to be 1 since the magnetic field is assumed to be not interacting in this phenomenon.

The reflection coefficient  $r$  at the interface between gold and prism is given by the equation,

$$r = \frac{R}{A} = \frac{(m'_{11} + m'_{12}q_3)q_1 - (m'_{21} + m'_{22}q_3)}{(m'_{11} + m'_{12}q_3)q_1 + (m'_{21} + m'_{22}q_3)}$$

where  $A$  and  $R$  are the amplitudes of the incident and the reflected electric field respectively.

The reflectivity which is the  $|r|^2$  is then plotted against  $\theta_1$ . This quantity reaches its minimum at the resonance angle where the energy from the incident electric field is mostly absorbed by the excited surface plasmon polaritons. While calculating the SPR angle we also consider the Fresnel coefficients at the prism-air interface at which the EM field enters and exits the prism. Thus we see the reflectivity for the deionized water reaches its minimum at the angle of 66 degrees and shifts towards right after the BSA binds the gold.

- 
- [1] Z. He, Y. Zhang, X. Tong, L. Li, and L. V. Wang, Quantum microscopy of cells at the heisenberg limit, *Nature Communications* **14**, 2441 (2023).
- [2] C. Lee, B. Lawrie, R. Pooser, K.-G. Lee, C. Rockstuhl, and M. Tame, Quantum plasmonic sensors, *Chemical Reviews* **121**, 4743 (2021).
- [3] M. S. Tame, K. McEnery, Ş. Özdemir, J. Lee, S. A. Maier, and M. Kim, Quantum plasmonics, *Nature Physics* **9**, 329 (2013).
- [4] V. Giovannetti, S. Lloyd, and L. Maccone, Quantum-enhanced measurements: beating the standard quantum limit, *Science* **306**, 1330 (2004).
- [5] W. Zhao, S. Zhao, L. Li, X. Huang, S. Xing, Y. Zhang, G. Qiu, Z. Han, Y. Shang, D.-e. Sun, *et al.*, Sparse deconvolution improves the resolution of live-cell super-resolution fluorescence microscopy, *Nature biotechnology* **40**, 606 (2022).
- [6] N. L. Thompson and B. L. Steele, Total internal reflection with fluorescence correlation spectroscopy, *Nature protocols* **2**, 878 (2007).
- [7] M. Gavutis, S. Lata, and J. Piehler, Probing 2-dimensional protein-protein interactions on model membranes, *Nature protocols* **1**, 2091 (2006).
- [8] K. M. Mayer and J. H. Hafner, Localized surface plasmon resonance sensors, *Chemical reviews* **111**, 3828 (2011).
- [9] J. N. Anker, W. P. Hall, O. Lyandres, N. C. Shah, J. Zhao, and R. P. Van Duyne, Biosensing with plasmonic nanosensors, *Nature materials* **7**, 442 (2008).
- [10] M. Soler, O. Calvo-Lozano, M. C. Estévez, and L. M. Lechuga, Nanophotonic biosensors: driving personalized medicine, (2020).
- [11] R. Karlsson, Spr for molecular interaction analysis: a review of emerging application areas, *Journal of Molecular Recognition* **17**, 151 (2004).
- [12] J.-F. Masson, Portable and field-deployed surface plasmon resonance and plasmonic sensors, *Analyst* **145**, 3776 (2020).
- [13] J.-F. Masson, Surface plasmon resonance clinical biosensors for medical diagnostics, *ACS sensors* **2**, 16 (2017).
- [14] H. M. Yang, J. Y. Teoh, G. H. Yim, Y. Park, Y. G. Kim, J. Kim, and D. Yoo, Label-free analysis of multivalent protein binding using bioresponsive nanogels and surface plasmon resonance (spr), *ACS applied materials & interfaces* **12**, 5413 (2020).
- [15] L. Jason-Moller, M. Murphy, and J. Bruno, Overview of biacore systems and their applications, *Current protocols in protein science* **45**, 19 (2006).
- [16] B. Douzi, Protein-protein interactions: surface plasmon resonance, *Bacterial Protein Secretion Systems: Methods and Protocols*, 257 (2017).
- [17] R. J. DeBerardinis and C. B. Thompson, Cellular metabolism and disease: what do metabolic outliers teach us?, *Cell* **148**, 1132 (2012).
- [18] K. Wanat, Biological barriers, and the influence of protein binding on the passage of drugs across them, *Molecular biology reports* **47**, 3221 (2020).
- [19] S. Schmidt, D. Gonzalez, and H. Derendorf, Significance of protein binding in pharmacokinetics and pharmacodynamics, *Journal of pharmaceutical sciences* **99**, 1107 (2010).
- [20] M. A. Zeitlinger, H. Derendorf, J. W. Mouton, O. Cars, W. A. Craig, D. Andes, and U. Theuretzbacher, Pro-

- tein binding: do we ever learn?, *Antimicrobial agents and chemotherapy* **55**, 3067 (2011).
- [21] Y. Phillip, V. Kiss, and G. Schreiber, Protein-binding dynamics imaged in a living cell, *Proceedings of the National Academy of Sciences* **109**, 1461 (2012).
- [22] X. Wang, M. Jefferson, P. C. Hobbs, W. P. Risk, B. E. Feller, R. D. Miller, and A. Knoesen, Shot-noise limited detection for surface plasmon sensing, *optics express* **19**, 107 (2010).
- [23] M. Piliarik and J. Homola, Surface plasmon resonance (spr) sensors: approaching their limits?, *Optics express* **17**, 16505 (2009).
- [24] A. A. Kolomenskii, P. Gershon, and H. Schuessler, Sensitivity and detection limit of concentration and adsorption measurements by laser-induced surface-plasmon resonance, *Applied optics* **36**, 6539 (1997).
- [25] K. C. Neuman, E. H. Chadd, G. F. Liou, K. Bergman, and S. M. Block, Characterization of photodamage to escherichia coli in optical traps, *Biophysical journal* **77**, 2856 (1999).
- [26] M. Dowran, A. Kumar, B. J. Lawrie, R. C. Pooser, and A. M. Marino, Quantum-enhanced plasmonic sensing, *Optica* **5**, 628 (2018).
- [27] M. Dowran, A. L. Win, U. Jain, A. Kumar, B. J. Lawrie, R. C. Pooser, and A. M. Marino, Parallel quantum-enhanced sensing, *ACS Photonics* **11**, 3037 (2024).
- [28] K. Mpofu and P. Mthunzi-Kufa, Enhanced signal-to-noise ratio in quantum plasmonic image sensing including loss and varying photon number, *Physica Scripta* **98**, 115115 (2023).
- [29] J.-S. Lee, S.-J. Yoon, H. Rah, M. Tame, C. Rockstuhl, S. H. Song, C. Lee, and K.-G. Lee, Quantum plasmonic sensing using single photons, *Optics express* **26**, 29272 (2018).
- [30] K. Mpofu, C. Lee, G. Maguire, H. Kruger, and M. Tame, Experimental measurement of kinetic parameters using quantum plasmonic sensing, *Journal of Applied Physics* **131** (2022).
- [31] R. C. Pooser and B. Lawrie, Plasmonic trace sensing below the photon shot noise limit, *ACS Photonics* **3**, 8 (2016).
- [32] O. Pluchery, R. Vayron, and K.-M. Van, Laboratory experiments for exploring the surface plasmon resonance, *European journal of Physics* **32**, 585 (2011).
- [33] C. McCormick, V. Boyer, E. Arimondo, and P. Lett, Strong relative intensity squeezing by four-wave mixing in rubidium vapor, *Optics letters* **32**, 178 (2007).
- [34] M. Kamble, J. Wang, and G. S. Agarwal, Quantum metrology of absorption and gain parameters using two-mode bright squeezed light, *Physical Review A* **109**, 053715 (2024).
- [35] F. Li, T. Li, M. O. Scully, and G. S. Agarwal, Quantum advantage with seeded squeezed light for absorption measurement, *Physical Review Applied* **15**, 044030 (2021).
- [36] T. Li, F. Li, X. Liu, V. V. Yakovlev, and G. S. Agarwal, Quantum-enhanced stimulated brillouin scattering spectroscopy and imaging, *Optica* **9**, 959 (2022).
- [37] C. McCormick, A. M. Marino, V. Boyer, and P. D. Lett, Strong low-frequency quantum correlations from a four-wave-mixing amplifier, *Physical Review A—Atomic, Molecular, and Optical Physics* **78**, 043816 (2008).